RSC Advances




ROYAL SOCIETY OF CHEMISTRY

www.rsc.org/advances

## Graphical Abstract

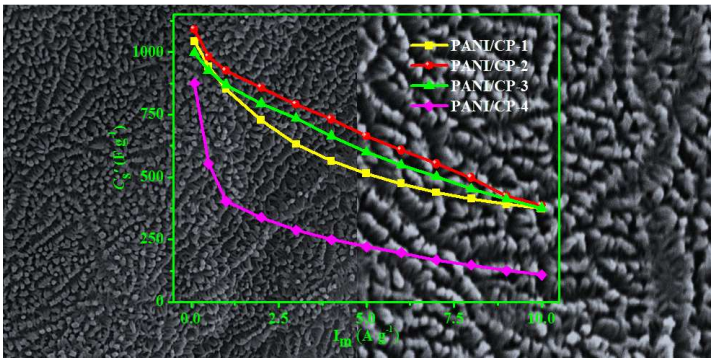


High performance supercapacitor is based on self-supported polyaniline/carbon paper composites derived from cellulose paper and in-situ polymerization of aniline.

Journal Name

RSCPublishing

ARTICLE

# Natural Source Derived Carbon Paper Supported Conducting Polymer Nanowire Arrays for High Performance Supercapacitors

Cite this: DOI: 10.1039/x0xx00000x

Received 00th January 2012,
Accepted 00th January 2012

DOI: 10.1039/x0xx00000x

www.rsc.org/

Chunxiang Hu,[a] Shuijian He,[a] Shaohua Jiang,[a*] Shuiliang Chen,[a] Haoqing Hou [a]*

Free-standing electrode materials have showed important application in supercapacitors. In this paper, a low cost and large scale producible carbon paper (CP) was prepared by the carbonization of cellulose paper. Self-supported conducting polymer composites were fabricated by in situ polymerization of aniline on the resulting CP substrate. The morphology and structure of as-prepared polyaniline/carbon paper (PANI/CP) composites were characterized by scanning electron microscope, transmission electron microscope, Fourier-transform infrared spectra and an automatic $N_2$ adsorption instrument. PANI/CP hybrids could be directly built into electrodes without adding polymer binders and conductive agents. The capacitance performance of PANI/CP electrodes was systematically studied with cyclic voltammetry, galvanostatic charge/discharge and electrochemical impedance spectroscopy. PANI/CP hybrids showed a high specific capacitance of 1090.8 F $g^{-1}$ along with low resistance and good stability. All the results indicated the prepared PANI/CP hybrids were promising electrode materials for supercapacitors.

## 1. Introduction

Supercapacitors or electrochemical capacitors have attracted more and more attention and are widely used in portable electronic devices, hybrid electric vehicles and backup sources due to their high power density, exceptional cycle life and faster charge-discharge rates.[1-4] According to the charge/discharge mechanisms, supercapacitors can be divided into electrical double-layer capacitors (EDLCs) and pseudocapacitors (PCs).[5] EDLCs based on high surface area carbon materials can obtain long cycle life (>$10^5$ cycles) but exhibit relatively low specific capacitance.[6-8] Compared with the EDLCs, PCs show much higher specific capacitance due to the superficial Faradaic reactions.[9, 10] Conducting polymers (polyaniline (PANI), polypyrrole, polythiophene and their derivatives) and transition metal compounds (oxides/hydroxides/sulfides) are major electrode materials for PCs.[11-16] Among these materials, PANI has been considered as one of the most promising candidates because of its facile synthesis, controllable nanostructures and high theoretical pseudocapacitance (>2000 F $g^{-1}$) among all the conducting polymers.[17-19] However, due to the volume change caused by the swelling and shrinkage during the $H^+$ doping/dedoping process accompanied with the charge-discharge process, pristine PANI electrode possesses poor cycling stability, which limits its application in the supercapacitors.[20]

Deposited PANI on carbon substrates, especially free-standing carbon frameworks, is proved to be an efficient approach to improve the capacitance performance of PANI.[21-25] Many research groups reported that using self-supported carbon materials including graphene foam/film/paper,[26-28] macroporous carbon,[29] carbon nanotubes,[30-32] electrospinning carbon nanofiber mats,[33-36] carbon foam,[37] commercial carbon fiber cloth,[38-41] carbon hybrids,[42-44] porous carbon nanofibers,[45] etc. as backbones to assemble free-standing PANI hybrids. As-prepared PANI composites can be fabricated into electrodes directly without the addition of polymer binders and conductive agents which decrease the "dead volume" and "dead weight" of the final devices. Moreover, these binder-free PANI composites always show enhanced rate performance and cycle stability compared to the pristine PANI and binder needed counterparts. However, most of self-supported carbon scaffolds are relatively high cost, low scale production and complicated in preparation, which considerably limit the large scale application of free-standing PANI/carbon composites for supercapacitors.

In recent years, papers made up by nature abundance cellulose have drawn much attention in fabricating free-standing devices for energy storage and other applications due to their low cost and good flexibility.[46-50] Moreover, cellulose paper can be converted to carbon paper (CP) by one step carbonization. The resulting CP is another type of self-supported conductive carbon substrate and have been successfully applied in supercapacitors.[51-53]

In this paper, we introduce a simple and cost-effective way to prepare free-standing PANI/CP composite for supercapacitor application. The PANI/CP composites were prepared by in situ polymerization of aniline nanowires on filter paper derived CP. The effect of sulfuric acid concentration on the morphology and electrochemical performance of resulting PANI/CP composite was investigated. Compared to other free-standing carbon frameworks,

these cellulose derived CP has advantages like simple preparation process and large scale productivity with low cost from cheap and abundant natural source. Moreover, the free-standing PANI/CP composites without any additional binders could considerably reduce the interface resistance. This free-standing PNAI/CP shows excellent capacitance performance with high specific capacitance, good rate capacitance and high stability and has potentially promising applications in energy storage devices with high power density and stability.

## 2. Experimental

### 2.1. Materials

Filter paper (FP) was purchased from Hangzhou Whoa filter paper Co. Ltd. Aniline (AN) (Shanghai Chem. Co) was distilled under reduced pressure and stored in dark prior to use. All the other chemicals were used as received.

### 2.2. Preparation of PANI/CP hybrids

Filter papers were first heated to 900 ºC at a rate of 5 ºC $min^{-1}$ under nitrogen atmosphere and hold for 2 h and then cooled down to room temperature to get carbon paper (CP). As-prepared CP was immersed in the concentrated sulfuric acid for 15 min to improve the hydrophilicity. The growth of PANI was carried out under nitrogen atmosphere in an ice-water bath. 0.2 g CP was first immersed into 0.2 L 10 mM AN aqueous solution with different sulfuric acid concentrations ($C_H$) for 0.5 h. After that 0.2 L 2.5 mM ammonium persulfate (APS) aqueous solution was added with rapid stirring. The polymerization was last for 4 h and then the composite papers were taken out and washed with 5% ammonia water, deionized water, absolute ethanol, and dimethyl sulfoxide (in sequence) until the filtrate was colorless and neutral. Finally the composite papers were dried under vacuum at 65 ºC. Series of PANI/CP electrodes were prepared from solutions with $C_H$ of 0.5 M, 1.5 M, 2.0 M and 3.0 M, respectively, and the composites were correspondingly marked as PANI/CP-1, PANI/CP-2, PANI/CP-3, and PANI/CP-4. The amount of PANI (PANI wt%) in the composite papers was calculated from the mass difference of samples before and after the polymerization.

### 2.3. Characterization

The morphology of the materials was characterized using a scanning electron microscope (SEM, TESCAN vega3) and transmission electron microscope (TEM, JEM-2010). Fourier-transform infrared spectra (FT-IR) of the samples were recorded with a Perkin Elmer 781 spectrophotometer. Surface and pore structure characterization of the materials were conducted with an automatic $N_2$ adsorption instrument (JW-K Gas Sorption Analyzer, JWGB Sci. and Tech. Co. Ltd., Beijing).

### 2.4. Electrode preparation and electrochemical measurements

The working electrodes were prepared by sandwiching pieces of the PANI/CP composite materials with the same weight between stainless steel mesh without any conductive additives and binders. All the electrochemical tests were carried out on a CHI660D electrochemical workstation (Shanghai Chenhua) in 1 M $H_2SO_4$ electrolyte. The cyclic voltammetry and electrochemical impedance spectroscopy (EIS) were carried out in a three-electrode system: a PANI/CP working electrode, a platinum wire counter electrode and an Ag/AgCl reference electrode (Sat. KCl). EIS was characterized in the frequency range from $10^5$ Hz to 0.01 Hz with the amplitude of 5 mV. Galvanostatic charge/discharge tests were carried out with two-electrode cell in the cut-off potential range of -0.2 to 0.6 V. The weight of the two electrodes was the same ($m = m_1 = m_2$). The specific capacitance ($C_s$) of the electrode was calculated from GCD curves by the equation:[54]

$$C_s = 2It/mV \qquad (1)$$

Where $I$ was the charge/discharge current ($A$), $t$ was the discharge time (s), m was the mass of the single electrode (g) and $V$ is the discharge voltage which did not include IR drop.

## 3. Results and discussion

### 3.1. Characterization of PANI/CP composites

The morphologies of CP and PANI/CP-2 are shown in **Fig. 1**. As showed in **Fig. 1a** and **1d**, the original CP shows smooth surface and is constituted by randomly connected carbon fragments with irregular shapes and carbon fibers with diameter in the range from a few to a dozen micrometers. The morphology of the CP changed a lot after in-situ polymerization of aniline. Take PANI/CP-2 for example, the surface of CP was covered by a uniform and ordered layer of PANI nanowire arrays (**Fig. 1b** and **1c**). The cross-section view of the composite paper revealed that PANI nanowires were coated on the entire surface of CP (**Fig. 1e**). PANI nanowires with length about 200-300 nm were solid and epitaxial grow from the surface of the CP as revealed by the TEM image (**Fig. 1f**).

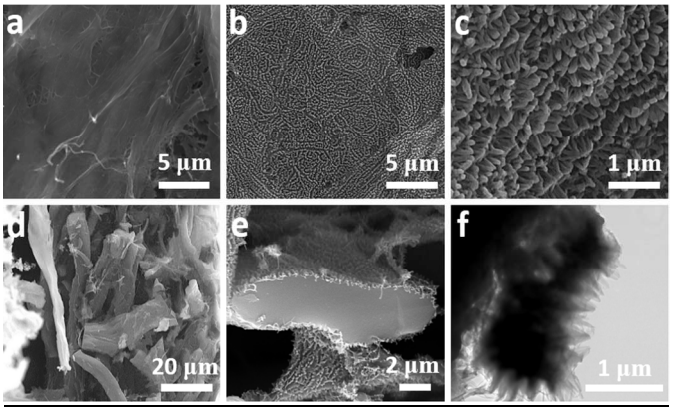


**Figure 1.** Top-view SEM images of the pristine CP (a) and the PANI/CP-2 composite (b and c). Cross-section view SEM images of the CP (d) and the PANI/CP-2 composite (e). TEM images of the PANI/CP-2 composite (f).

The properties of the PANI nanomaterials were influenced by many issues including the type of acid used, the molar ratio of oxidant to monomer, reaction temperature and time, etc.[55] In this work, the effect of sulfuric acid concentration ($C_H$) on the morphology and capacitance performance of PANI/CP composite papers was studied. The $C_H$ was varied from 0.5 M to 3.0 M in our experiments and the SEM images of resulting composites were displayed in **Fig 2**. When the applied $C_H$ was 0.5 M, short and round PANI nanowires were covered over the CP (**Fig. 2**a and e). As the $C_H$ increase to 1.5 M, longer PANI nanowires (Length: 263 ± 20 nm) with an ordered structure were observed (**Fig. 2**b and f), which ensured the effective electrolyte transportation. However, further increase of $C_H$ to 2.0 M and 3.0 M led to thicker layer of much denser PANI nanowire arrays covered onto the CP (**Fig. 2**c, g and d, h) and the length of the PANI nanowires decreased to 187 ± 25 nm and 138 ± 17 nm, respectively.



 

These denser and shorter PANI nanowires around the CP were unfavorable for rapid electrolyte diffusion and full utilization of PANI.

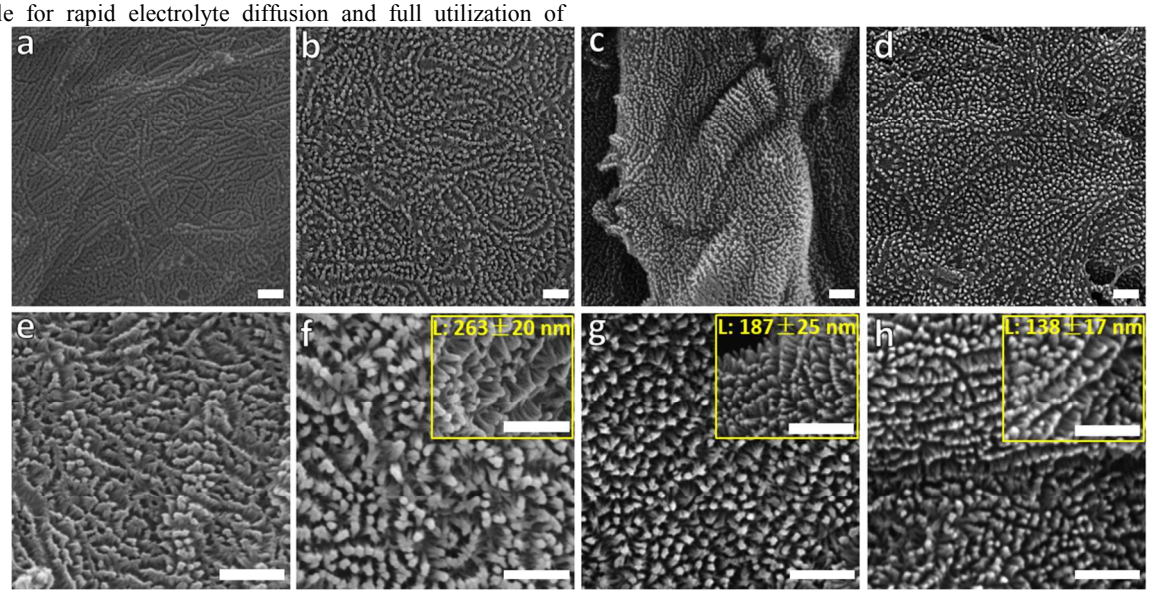


**Figure 2.** SEM images of PANI/CP composites prepared from different $H_2SO_4$ concentration of 0.5 M (a, e), 1.5 M (b, f), 2.0 M (c, g) and 3.0 M (d, h). Insert photos of (f), (g) and (h) showed the length of PANI nanowires. Scale bar = 1 μm.

FT-IR spectrum of PANI/CP-2 is showed in **Fig. 3**. The characteristic peaks at the 1571 and 1482 $cm^{-1}$ are attributed to the C=C stretching vibrations of the quinoid and benzenoid rings, respectively. The bands at the 1305 $cm^{-1}$ and 1211 $cm^{-1}$ correspond to the C-N and C-N-C stretching vibrations of PANI, respectively.[56] The characteristic band observed at the 1137 $cm^{-1}$ (N=Q=C) corresponds to the polyaniline salt.[57] The presence of above bands indicated that the PANI was successfully polymerized around the surface of the CP.

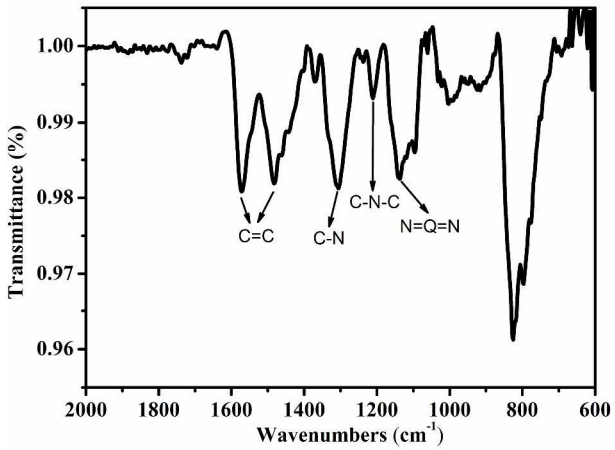


**Figure 3.** FT-IR spectra of PANI/CP-2 composite.

Porous characteristics, including specific surface area ($S_A$), pore volume ($V_t$) and pore size distribution, were tested by the automatic $N_2$ adsorption measurements and the results are displayed in **Fig. 4** and **Table 1**. The $S_A$ and $V_t$ decreased after the growth of PANI. The results of the pore size distribution (**Fig. 4**) revealed that after the growth of PANI, the nano-sized pores of CP were mostly filled or plugged by the PANI. This phenomenon was similar to the other polyaniline/porous carbon composites.[58-61] The $S_A$ and $V_t$ of the PANI/CP composites reached the maximum value when $C_H$ was 1.5 M. The PANI/CP-2 showed the highest $S_A$ of 12.26 $m^2$ $g^{-1}$ and $V_t$ of 0.039 $cm^3$ $g^{-1}$ due to the relative thinner PANI layer and the largest length of the PANI nanowires on the CP (**Fig. 2**).

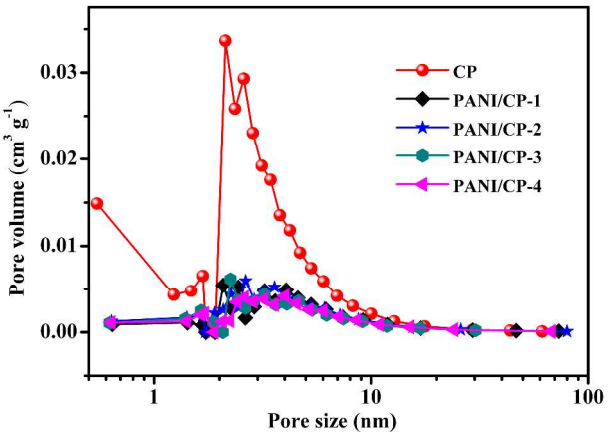


**Figure 4.** Pore size distribution of CP and PANI/CP electrodes.

### 3.2. Electrochemical characteristics

To evaluate the electrochemical capacitance performance of PANI/CP composites, cyclic voltammetry (CV), galvanostatic charge/discharge (GCD) and electrochemical impedance spectroscopy (EIS) were performed on a CHI660D electrochemical workstation. CV curves at a scan rate of 10 mV $s^{-1}$ were exhibited in **Fig. 5**. The CP electrode was also tested for comparison. The integral areas of the CV curves showed that the CP substrate exhibited negligible capacitance when compared to the PANI/CP composites. Therefore, the capacitances of the PANI/CP composites could be considered mainly contributed from the pesudocapacitance of the PANI nanowire arrays and the CP acted only as the conductive substrate. Thus, the weight of the carbon paper was not taken into account for the specific capacitance calculation. Two couples of redox peaks ($O_1/R_1$, $O_2/R_2$) appeared in the CV curves of

the PANI/CP electrodes, which could be attributed to the redox transitions (semiconducting state and conducting states) of the PANI, and the transformation of the emeraldine-pernigraniline.[62, 63] Among the PANI/CP composite electrodes, PANI/CP-2 presented a higher current density and larger integral area indicating PANI/CP-2 owned an optimal specific capacitance.

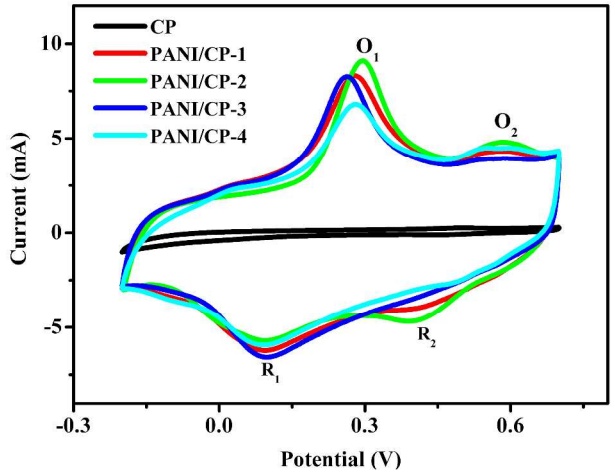


**Figure 5.** The CV curves of PANI/CP and CP electrodes at a scan rate of 10 mV $s^{-1}$.

The GCD tests were further carried out to reveal the detailed electrochemical performance of the composite materials. **Fig. 6** showed the charge/discharge curves of the PANI/CP electrodes at a constant current density of 0.1 and 1 A $g^{-1}$. All the charge/discharge curves were symmetric which indicated a reversible behavior required for ideal capacitors at 0.1 A $g^{-1}$. When current density of 1 A $g^{-1}$ was applied, the composite electrodes of PANI/CP-1, PANI/CP-2 and PANI/CP-3 still exhibited symmetric charge/discharge curves. However, the sample PANI/CP-4 showed asymmetric charge/discharge curve at 1 A $g^{-1}$, which could be due to the much higher internal resistance of the largest amount of PANI compared to other PANI/CP composites. In addition, the deviation from the linearity revealed the capacitance of PANI/CP composites mainly originated from the pseudocapacitance.

**Fig. 5** showed that the specific capacitance of CP is far less than those of PANI/CP composites. Therefore, in the following part, the weight of the CP was not taken into account for the specific capacitance ($C_s'$) calculation of active material PANI. The specific capacitance ($C_s'$), energy density $W$ (Wh $kg^{-1}$) and power density $P$ (kW $kg^{-1}$) of the active material of PANI in a single electrode were calculated according to the following equations:[64]

$$C_s' = C_s/\omega \qquad (2)$$

$$W = 0.5 \times C_s' \times V^2 \qquad (3)$$

$$P = W/t \qquad (4)$$

Where $t$ was the discharge time (s), ω is the weight percentage (wt%) of the active material (PANI) in a single electrode and $V$ is the discharge voltage which did not include IR drop. The $C_H$ dependence of the amount of PANI (PANI wt%) and $C_s'$ was shown in **Table 1**. The PANI wt% increased with the increase of $C_H$ in the range from 0.5 to 3.0 M. $C_s'$ reached 1043.2, 1090.8, 997.5 and 874.6 F $g^{-1}$ at current density of 0.1 A $g^{-1}$ for PANI/CP-1, PANI/CP-2, PANI/CP-3 and PANI/CP-4, respectively. The $C_s'$ were comparable to or even surpassed the values of other self-standing PANI composites.[28, 35, 40, 49, 65, 66] Although PANI/CP-3 and PANI/CP-4 had higher PANI wt%, their $C_s'$ were lower than that of the PANI/CP-2. This was because the thicker and tightly cumulated PANI layer on the CP hindered the electrolyte diffusion into the interior of PANI layer. The highest $C_s'$ displayed by the PANI/CP-2 composites could be explained by the following reasons. First, the 3D self-supported CP substrate could avoid the use of binders and thus guaranteed the full utilization of PANI nanowires. Second, the composite showed three dimension hierarchical porous structure comprising micrometer size large spaces among carbon species and "V-type" nanochannels among PANI nanowires. Such porous structure was able to hold a large amount of electrolyte and shortened electrolyte diffusion path.[62] Third, PANI/CP-2 composites possessed optimized thickness, appropriate density, highest specific surface area and the largest length of PANI nanowires.

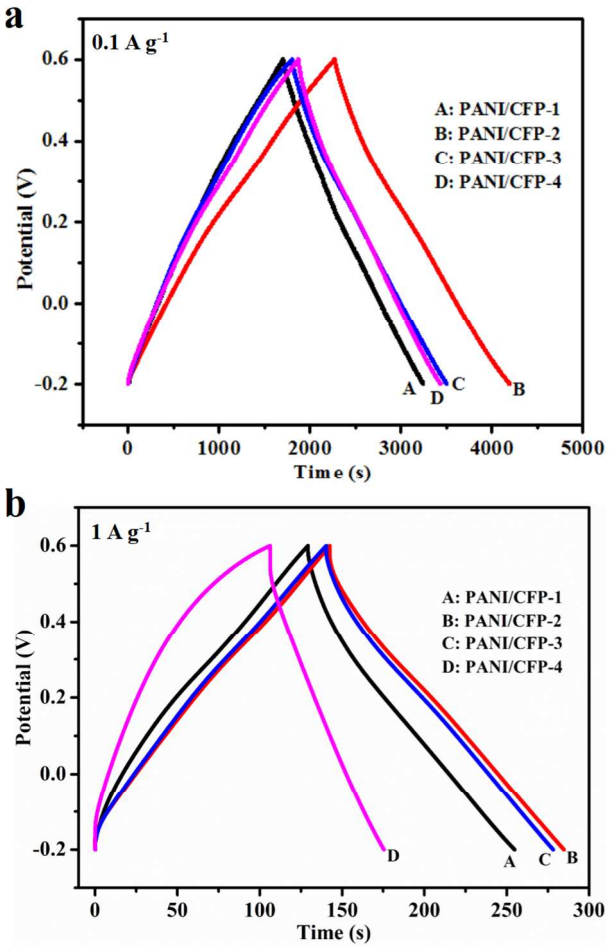


**Figure 6.** Galvanostatic charge/discharge curves of PANI/CP electrodes at current densities of (a) 0.1 A $g^{-1}$ and (b) 1 A $g^{-1}$.

**Table 1.** Characteristics of CP and PANI/CP composites.

| Sample | $C_H$ (M) | $S_A$ ($m^2$ $g^{-1}$) | $V_t$ ($cm^3$ $g^{-1}$) | $m_{PANI}$ (mg) | PANI (wt%) | $C_s$ | $C_s'$ |
|---|---|---|---|---|---|---|---|
| CP | - | 51.65 | 0.097 | 0 | 0 | - | - |
| PANI/CP-1 | 0.5 | 11.62 | 0.038 | 0.3748 | 18.74 | 195 | 1043.2 |

| | | | | | | | |
|---|---|---|---|---|---|---|---|
| PANI/CP-2 | 1.5 | 12.26 | 0.039 | 0.3908 | 19.54 | 240 | 1090.8 |
| PANI/CP-3 | 2.0 | 8.72 | 0.032 | 0.4024 | 20.12 | 213 | 997.5 |
| PANI/CP-4 | 3.0 | 8.18 | 0.033 | 0.4418 | 22.09 | 200 | 874.6 |

Note: specific surface area ($S_A$), pore volume ($V_t$), specific capacitance ($C_s$) of the PANI/CP electrode, specific capacitance ($C_s'$) of the active material of PANI in a single electrode at 0.1 A $g^{-1}$.

**Fig. 7**a revealed the relationship of the specific capacitance and the current density. All the PANI/CP electrodes displayed decreased $C_s'$ with the increase of discharge current density due to limited redox reaction rate of PANI. The $C_s'$ of PANI/CP-2 retained 386.9 F $g^{-1}$ when current density increased 100 folds from 0.1 A $g^{-1}$ to 10 A $g^{-1}$ indicating the good rate capacitance performance. The Ragone plots showed that the PANI/CP electrodes could work in wide power ranges with relatively high energy densities (**Fig. 7**b). The energy density of the PANI/CP-2 achieved 94.2 Wh $kg^{-1}$ at a power density of 0.2 kW $kg^{-1}$ and still retained 34.0 Wh $kg^{-1}$ when power density increased to 22.0 kW $kg^{-1}$, indicating the excellent rate performance and hig power density of the PANI/CP composites.

EIS analysis is an effective approach to evaluate the conductivity, structure and charge transport properties of electrode materials. The resulting Nyquist plots were shown in **Fig. 7**c. Each Nyquist plot showed a semicircle in the high frequency area and a near vertical line in the low frequency area. At the low frequency area, the vertical degree of straight line represented purity of the capacitive behavior. At the high frequency area, the semicircle was related to the charge-transfer resistance and the charge transfer resistance can be calculated form the diameter of the semicircle. The PANI/CP-2 electrode showed the most vertical curve in the low frequency area and a smallest semicircle in the high frequency area in all the PANI/CP composites, indicating a better capacitive behavior and a lower charge-transfer resistance, respectively. The charge transfer resistance of PANI/CP electrodes was 5.5, 4.2，8.2 and 12.4 Ω for the PANI nanowires deposited from $C_H$ of 0.5, 1.5, 2.0 and 3.0 M, respectively. The increase in the resistance could be attributed to the increase in PANI nanowire density and PANI layer thickness.

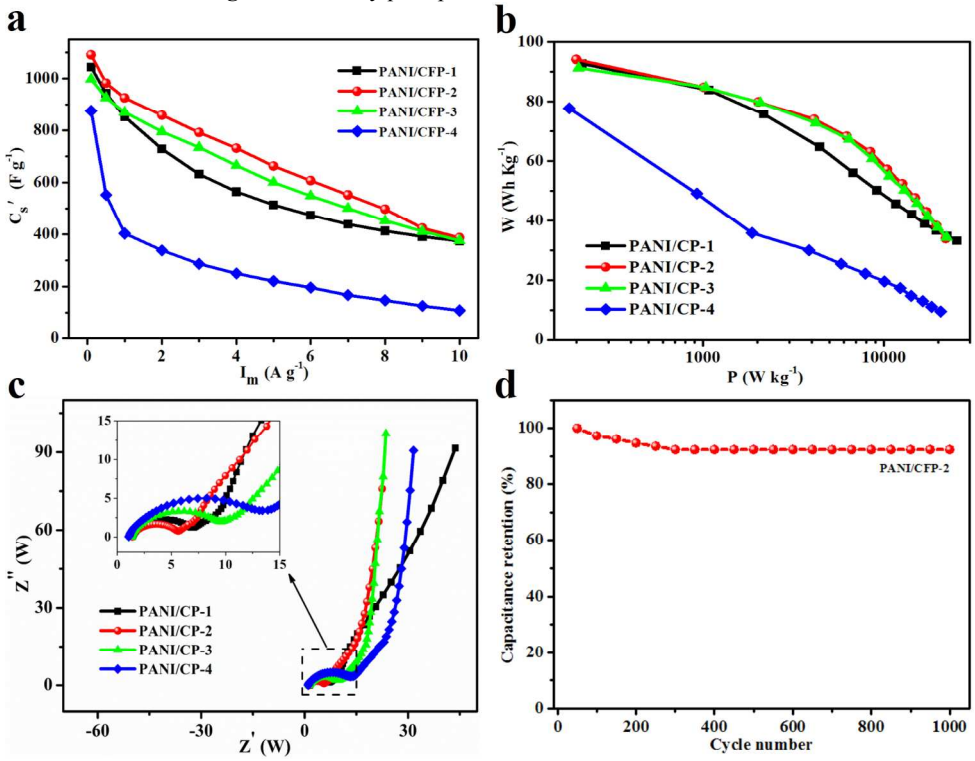


**Figure 7.** Specific capacitance plots at different current densities (a), Ragone plots (b), Nyquist plots of supercapacitors based on the PANI/CP electrodes (c) and plots of cycle life test of PANI/CP-2 electrodes at current density of 10 A $g^{-1}$ (d).

The cycling stability was another important parameter in evaluating the performance of supercapacitor electrode materials. As shown in **Fig. 7**d, PANI/CP-2 showed excellent cycle performance even been tested under a much high current density of 10 A $g^{-1}$. After 1000 cycles, the $C_s'$ of PANI/CP-2 electrode still remained about 84%. The 16% loss of $C_s'$ could be come from the ineffective contact between the unstable PANI and CP, as well as the subsequent deterioration of the electron transfer and ion diffusion pathway.[23, 38, 52] In the other hand, the excellent cycle stability could be attributed to the advantages that the PANI nanowires on the skeletal CP substrate could effectively overcome the swelling and shrinkage drawbacks during doping/dedoping processes.[67]

## 4. Conclusions

In summary, we fabricated a series of PANI/CP composites with 3D micro/nano hierarchical structures by in-situ polymerization of aniline onto the cellulose paper derived carbon paper. The resulting composite electrodes, without adding any binders and conducting additives could be directly fabricated into supercapacitors. The influence of sulfuric acid concentration ($C_H$) on the morphology and

capacitance performance of PANI/CP composite papers was studied. When the $C_H$ was 1.5 M, the resulting PANI/CP-2 possessed the highest specific capacitance of 1090.8 F $g^{-1}$ at 0.1 A $g^{-1}$. This study provided a simple, low-cost and facile method to prepare CP based self-supported PANI composites. The composites displayed outstanding capacitance performance and could be used as the promising electrode material for the supercapacitors.

## Acknowledgements

This work is supported by the National Natural Science Foundation of China (Grants No.: 21174058 & No.: 21374044), the Major Special Projects of Jiangxi Provincial Department of Science and Technology (Grant No.: 20114ABF05100) and the Technology Plan Landing Project of Jiangxi Provincial Department of Education.

### Notes and references

[a] Chemistry and Chemical Engineering College, Jiangxi Normal University, Nanchang, Jiangxi 330022, P.R. China; Tel: +86 791 88120740 E-mail: s.jiang19830913@gmail.com and haoqing@jxnu.edu.cn

1. P. Simon and Y. Gogotsi, *Nature materials*, 2008, **7**, 845-854.
2. P. J. Hall, M. Mirzaeian, S. I. Fletcher, F. B. Sillars, A. J. R. Rennie, G. O. Shitta-Bey, G. Wilson, A. Cruden and R. Carter, *Energy Environ. Sci.*, 2010, **3**, 1238-1251.
3. Q. Zhang, E. Uchaker, S. L. Candelaria and G. Cao, *Chem. Soc. Rev.*, 2013, **42**, 3127-3171.
4. S.-M. Chen, R. Ramachandran, V. Mani and R. Saraswathi, *Int. J. Electrochem. Sci*, 2014, **9**, 4072-4085.
5. G. Wang, L. Zhang and J. Zhang, *Chem. Soc. Rev.*, 2012, **41**, 797-828.
6. M. D. Stoller and R. S. Ruoff, *Energy Environ. Sci.*, 2010, **3**, 1294-1301.
7. M. Winter and R. J. Brodd, *Chem. Rev.*, 2004, **104**, 4245-4269.
8. V. Subramanian, H. Zhu, R. Vajtai, P. Ajayan and B. Wei, *J. Phys. Chem. B*, 2005, **109**, 20207-20214.
9. Y. Zhang, H. Feng, X. Wu, L. Wang, A. Zhang, T. Xia, H. Dong, X. Li and L. Zhang, *Int. J. Hydrogen Energy*, 2009, **34**, 4889-4899.
10. L. L. Zhang and X. Zhao, *Chem. Soc. Rev.*, 2009, **38**, 2520-2531.
11. G. A. Snook, P. Kao and A. S. Best, *J. Power Sources*, 2011, **196**, 1-12.
12. N. Ashok Kumar and J.-B. Baek, *Chem. Commun.*, 2014, **50**, 6298-6308.
13. M. R. Gao, Y. F. Xu, J. Jiang and S. H. Yu, *Chem. Soc. Rev.*, 2013, **42**, 2986-3017.
14. J. Jiang, Y. Y. Li, J. P. Liu, X. T. Huang, C. Z. Yuan and X. W. Lou, *Adv. Mater.*, 2012, **24**, 5166-5180.
15. J. P. Cheng, J. Zhang and F. Liu, *Rsc Advances*, 2014, **4**, 38893-38917.
16. W. T. Deng, X. B. Ji, Q. Y. Chen and C. E. Banks, *RSC Advances*, 2011, **1**, 1171-1178.
17. L. Li, J. Qiu and S. Wang, *Electrochim. Acta*, 2013, **99**, 278-284.
18. J. Xu, K. Wang, S.-Z. Zu, B.-H. Han and Z. Wei, *Acs Nano*, 2010, **4**, 5019-5026.
19. H. Li, J. Wang, Q. Chu, Z. Wang, F. Zhang and S. Wang, *J. Power Sources*, 2009, **190**, 578-586.
20. S. He, X. Hu, S. Chen, H. Hu, M. Hanif and H. Hou, *J. Mater. Chem.*, 2012, **22**, 5114-5120.
21. Y. N. Meng, K. Wang, Y. J. Zhang and Z. X. Wei, *Adv. Mater.*, 2013, **25**, 6985-6990.
22. H. S. Fan, N. Zhao, H. Wang, J. Xu and F. Pan, *J. Mater. Chem. A*, 2014, **2**, 12340-12347.
23. H.-P. Cong, X.-C. Ren, P. Wang and S.-H. Yu, *Energy Environ. Sci.*, 2013, **6**, 1185-1191.
24. C. Peng, S. Zhang, D. Jewell and G. Z. Chen, *Progress in Natural Science*, 2008, **18**, 777-788.
25. R. Ramya, R. Sivasubramanian and M. V. Sangaranarayanan, *Electrochim. Acta*, 2013, **101**, 109-129.
26. Y. Z. Xie, Y. Liu, Y. D. Zhao, Y. H. Tsang, S. P. Lau, H. T. Huang and Y. Chai, *J. Mater. Chem. A*, 2014, **2**, 9142-9149.
27. D. D. Xu, Q. Xu, K. X. Wang, J. Chen and Z. M. Chen, *ACS Appl. Mat. Interfaces*, 2014, **6**, 200-209.
28. P. Yu, X. Zhao, Z. Huang, Y. Li and Q. Zhang, *J. Mater. Chem. A*, 2014, **2**, 14413-14420.
29. L. L. Zhang, S. Li, J. Zhang, P. Guo, J. Zheng and X. S. Zhao, *Chem. Mater.*, 2009, **22**, 1195-1202.
30. F. Huang, F. Lou and D. Chen, *ChemSusChem*, 2012, **5**, 888-895.
31. A. Ul Haq, J. Lim, J. M. Yun, W. J. Lee, T. H. Han and S. O. Kim, *Small*, 2013, **9**, 3829-3833.
32. Z. Niu, P. Luan, Q. Shao, H. Dong, J. Li, J. Chen, D. Zhao, L. Cai, W. Zhou, X. Chen and S. Xie, *Energy Environ. Sci.*, 2012, **5**, 8726-8733.
33. Z. P. Zhou, X. F. Wu and H. Q. Hou, *RSC Advances*, 2014, **4**, 23622-23629.
34. S. J. He, X. W. Hu, S. L. Chen, H. Hu, M. Hanif and H. Q. Hou, *J. Mater. Chem.*, 2012, **22**, 5114-5120.
35. Z. Zhou and X.-F. Wu, *J. Power Sources*, 2014, **262**, 44-49.
36. Z. Zhou, X.-F. Wu and H. Hou, *RSC Advances*, 2014, **4**, 23622-23629.
37. H. Hu, S. Liu, M. Hanif, S. Chen and H. Hou, *J. Power Sources*, 2014, **268**, 451-458.
38. Q. Cheng, J. Tang, J. Ma, H. Zhang, N. Shinya and L.-C. Qin, *J. Phys. Chem. C*, 2011, **115**, 23584-23590.
39. P. Yu, Y. Li, X. Yu, X. Zhao, L. Wu and Q. Zhang, *Langmuir*, 2013.
40. P. P. Yu, Y. Z. Li, X. Zhao, L. H. Wu and Q. H. Zhang, *Langmuir*, 2014, **30**, 5306-5313.
41. P. Yu, Y. Li, X. Yu, X. Zhao, L. Wu and Q. Zhang, *Langmuir*, 2013, **29**, 12051-12058.
42. D. Xu, Q. Xu, K. Wang, J. Chen and Z. Chen, *ACS Appl. Mat. Interfaces*, 2013, **6**, 200-209.
43. G. Ning, T. Li, J. Yan, C. Xu, T. Wei and Z. Fan, *Carbon*, 2013, **54**, 241-248.
44. G. Xu, C. Zheng, Q. Zhang, J. Huang, M. Zhao, J. Nie, X. Wang and F. Wei, *Nano Research*, 2011, **4**, 870-881.
45. M. Dirican, M. Yanilmaz and X. Zhang, *RSC Advances*, 2014, **4**, 59427-59435.
46. Z. Weng, Y. Su, D. W. Wang, F. Li, J. Du and H. M. Cheng, *Advanced Energy Materials*, 2011, **1**, 917-922.
47. L. Hu, J. W. Choi, Y. Yang, S. Jeong, F. La Mantia, L. F. Cui and Y. Cui, *Proceedings of the National Academy of Sciences*, 2009, **106**, 21490-21494.
48. J. W. Han, B. Kim, J. Li and M. Meyyappan, *Mater. Res. Bull.*, 2014, **50**, 249-253.
49. L. L. Liu, Z. Q. Niu, L. Zhang, W. Y. Zhou, X. D. Chen and S. S. Xie, *Adv. Mater.*, 2014, **26**, 4855-4862.
50. B. Yao, L. Yuan, X. Xiao, J. Zhang, Y. Qi, J. Zhou, J. Zhou, B. Hu and W. Chen, *Nano Energy*, 2013, **2**, 1071-1078.
51. S. He, C. Hu, H. Hou and W. Chen, *J. Power Sources*, 2014, **246**, 754-761.
52. M. Liu, S. He, W. Fan, Y.-E. Miao and T. Liu, *Compos. Sci. Technol.*, 2014, **101**, 152-158.
53. C. Hu, Y. He, S. Chen, Y. Zhu, M. Hanif and H. Hou, *J. Solid State Electrochem.*, 2014, **18**, 2797-2802.



 

54. Z. Xu, Z. Li, C. M. B. Holt, X. Tan, H. Wang, B. S. Amirkhiz, T. Stephenson and D. Mitlin, *The Journal of Physical Chemistry Letters*, 2012, **3**, 2928-2933.
55. S. Bhadra, D. Khastgir, N. K. Singha and J. H. Lee, *Prog. Polym. Sci.*, 2009, **34**, 783-810.
56. Y. Li, Y. Z. Fang, H. Liu, X. M. Wu and Y. Lu, *Nanoscale*, 2012, **4**, 2867-2869.
57. F. Yang, M. W. Xu, S. J. Bao and Q. Q. Sun, *RSC Advances*, 2014, **4**, 33569-33573.
58. Z. B. Lei, Z. W. Chen and X. S. Zhao, *Journal of Physical Chemistry C*, 2010, **114**, 19867-19874.
59. L. P. Zheng, Y. Wang, X. Y. Wang, N. Li, H. F. An, H. J. Chen and J. Guo, *J. Power Sources*, 2010, **195**, 1747-1752.
60. H. F. An, Y. Wang, X. Y. Wang, N. Li and L. P. Zheng, *J. Solid State Electrochem.*, 2009, **14**, 651-657.
61. A. A. Ali and G. C. Rutledge, *J. Mater. Process. Technol.*, 2009, **209**, 4617-4620.
62. Y. G. Wang, H. Q. Li and Y. Y. Xia, *Adv. Mater.*, 2006, **18**, 2619-2623.
63. L. Yuan, X. Xiao, T. Ding, J. Zhong, X. Zhang, Y. Shen, B. Hu, Y. Huang, J. Zhou and Z. L. Wang, *Angew. Chem.*, 2012, **124**, 5018-5022.
64. S. J. He and W. Chen, *J. Power Sources*, 2014, **262**, 391-400.
65. S. He, J. Wei, F. Guo, R. Xu, C. Li, X. Cui, H. Zhu, K. Wang and D. Wu, *J. Mater. Chem. A*, 2014, **2**, 5898-5902.
66. C. Xia, Y. Xie, W. Wang and H. Du, *Synth. Met.*, 2014, **192**, 93-100.
67. H. Cao, X. Zhou, Y. Zhang, L. Chen and Z. Liu, *J. Power Sources*, 2013, **243**, 715-720.